

IDENTIFICATION OF FLOODPLAIN AND RIVERBED SEDIMENT HETEROGENEITY IN
A MEANDERING UK LOWLAND STREAM BY GROUND PENETRATING RADAR

Rebwar Dara^{1,2,*} rebwar.nasir@gmail.com, Nicholas Kettridge¹, Michael O. Rivett³, Stefan.
Krause¹, David Gomez-Ortiz⁴

¹School of Geography, Earth and Environmental Sciences, University of Birmingham, Edgbaston,
Birmingham, B15 2TT, UK

²Knowledge University, College of Engineering, Department of Environmental Engineering –
Kurdistan region- Erbil, Iraq

³Civil and Environmental Engineering, University of Strathclyde, 16 Richmond St, Glasgow, G1
1XQ, UK

⁴Dpt. Biología y Geología, Física y Química Inorgánica, ESCET, Universidad Rey Juan Carlos,
C/Tulipán s/n, 28933 Móstoles, Madrid, Spain

*Corresponding author.

Abstract

Complex spatial heterogeneity in riverbed and floodplain sediments control the spatio-temporal exchange of groundwater and surface water in the hyporheic zone, inducing hot spots of microbial activity and biogeochemical cycling. However, the characterization of hyporheic exchange dynamics has thus far failed to adequately account for the complex subsurface heterogeneity of river bed sediments in a spatially explicit manner, in particular for highly complex lowland river bed sediments. Here we demonstrate the ability of ground penetrating radar (GPR) to efficiently map floodplain and river bed sediment structures within a lowland meandering river. The aim of this study was to delineate the type and spatial extent of complex, texturally heterogeneous facies of high and low conductive streambed materials. GPR surveys in this study involved not only state-of-the-art terrestrial applications but also an aquatic survey conducted from a floating rig. The surveys revealed substantial sub-surface heterogeneity of depositional materials in the streambed and riparian zone. Eight characteristic radar facies were identified through the floodplain and ground-truthed against core samples and exposures of bank deposits. The majority of GPR profiles were dominated by trough-shaped depositional elements with erosional, curved, concave upward bounding surfaces, indicative of abandoned and chute stream channel structures. The identified abandoned channel structure was found to extend into the riverbed and to be filled by suspension fall-out fine-grained deposits (mud with organic matter and interbedded clay as indicated by observed signal attenuations). GPR proved to be a successful method to identify the spatial patterns of low conductivity peat and clay structures in the streambed and riparian zone of the investigated meander bend, highlighting its potential for larger scale analysis of these structures that have shown to control the exchange flow patterns between groundwater and surface water in lowland rivers.

Keywords: Ground penetrating radar (GPR), Lowland meandering, Ground-truth, permeability field, Radar facies, Hydrogeological model

1. Introduction

Alluvial valleys are characterised by the existence of complex spatial patterns of hydraulic conductivities, resulting from their history of erosion and deposition in the valley that operated in different palaeo-geomorphic environments (Kostic and Aigner, 2007a; Tonina and Buffington, 2009). Variability in alluvial sediments usually ranges from decimetre-to-metre scale, spanning several orders of magnitude in hydraulic conductivity (K) (Miall, 1996; Krause et al., 2013). Further, the deposition of fine particles (clay and silt) and organic matter in alluvial sediments can substantially reduce the permeability of riverbed sediments and extend towards the wider floodplain (Tonina and Buffington, 2009; Wondzell and Gooseff, 2013). Detailed knowledge of sediment property distributions and specifically spatial heterogeneity of the permeability field in streambed and riparian sediments are crucial for better understanding and predicted shallow groundwater flow and recharge in floodplains as well as groundwater – surface water exchange flow patterns across multiple spatial scales (Beres and Haeni, 1991; Huggenberger, 1993; Beres et al., 1995; Conant, 2004; Krause et al., 2012b).

Spatial patterns of hydraulic conductivities within streambed and floodplain have been shown to control both location and intensity of hyporheic exchange (Fleckenstein et al., 2006; Krause et al., 2009b; Cardenas and Jiang, 2010; Krause et al., 2012b; Gomez-Velez et al., 2014) as well as larger scale groundwater and surface water interactions (including substantial bank storage) in many lowland rivers (Naranjo et al., 2012; Binley et al., 2013). Furthermore, recent modelling studies evidence that knowledge of the location and spatial extent of contrasting hydrofacies is essential to understanding and predicting patterns and intensities of groundwater and surface water exchange and in particular hyporheic exchange fluxes (Gomez-Velez et al., 2014; Trauth and Fleckenstein 2017).

Invasive approaches to determine sediment permeability and the spatial extent of identified low conductivity features relevant to groundwater and surface water exchange, such as core drillings or the sampling and analysis of bank exposures, are expensive and time-consuming and potentially alter the investigated conditions (Binley et al., 2015). These more traditional methods provide limited spatial information on hydrological properties and are often unsuitable to make adequate assumptions about the spatial complexity of alluvial sediment systems required to support a comprehensive hydrogeological characterization (Clifford and Binley, 2010). Furthermore, invasive approaches prevent or at least limit re-occurring analysis since they modify the subject of

investigation, which is of particular importance for temporally less stationary structures such as riverbed sediments (Krause et al., 2012b).

The development of near-surface geophysical analysis tools over the last decades has opened unprecedented opportunities for larger scale, high resolution characterisation of subsurface structural complexity and hydrological functioning units (hydrofacies) in order to better understand the geological and geomorphological controls on riparian flow systems and groundwater and surface water exchange flow patterns (Salehin et al., 2004; Fleckenstein et al., 2006; Krause et al., 2012b). A wide range of geophysical methods (e.g. electrical methods, electromagnetic induction (EM), and ground penetrating radar (GPR)) have been trialed and applied to investigate the spatial complexity of alluvial deposits (Conant et al., 2004; Crook et al., 2008; Binley et al., 2015). Near surface geoelectrical methods such as vertical electrical soundings (VES) and electrical resistivity tomography (ERT) have been regularly applied for hydrogeological applications (Daily and Ramirez, 2000; Reynolds, 2011). However, due to their limitation with accurately resolving lithological boundaries between hydrofacies (Bersezio et al., 2007) and strategic difficulties for setting up larger scale in-stream surveys in particular, they have not been applied frequently for characterising complex hydrofacies distributions in riparian zones and streambed environments (Naden, 2011).

Ground penetrating radar (GPR) refers to a non-invasive method which is designed mainly for subsurface investigations (Neal, 2004; Cassidy and Jol, 2009). GPR can detect changes in dielectric properties of the shallow subsurface using high frequency electromagnetic (EM) waves in the range of 10-1000 MHz (Neal, 2004). The high spatial resolution at higher measurement frequencies, the detection of boundaries and the rapid measurement times represent important reasons why GPR is frequently used in to characterize hydrofacies (e.g. Topp et al., 1980; van Dam and Schlager, 2000). However, it is widely acknowledged that low conductivity layers can excessively attenuate GPR signals, while reducing the depth of penetration (Theimer et al., 1994; Heteren et al., 1998; Bristow and Jol, 2003). This condition can be used, of course, to identify alluvial fill thicknesses for instance (Leclerc and Hickin, 1997). Compared with EM-based techniques, including resistivity surveying, GPR offers advantages due to its relative insensitivity to changes in pore water chemistry, and its provision of high resolution images that enable a clearer interpretation of GPR results (Binley et al., 2001).

GPR has been used previously to characterize fluvial sediments in floodplains (e.g. Bridge et al. 1995; Leclerc and Hickin, 1997; Vandenberghe and van Overmeeren, 1999; Gourry et al., 2003; Skelly et al., 2003; Lunt et al., 2004; Kostic and Aigner, 2007b; Hickin et al., 2009; Rice et al., 2009; Ashworth et al., 2011; Słowik, 2013b; Reesink et al., 2014, among others). However, GPR applications in streams are rare and technologically challenging. Naegeli et al. (1996) used GPR in river channels to investigate the sediment structures in a flood-prone gravel-bed River. Conant et al. (2004) have also used GPR successfully to delineate potential preferential pathways of sandy channel infill deposits and semi-confining units that control the rates and distribution of PCE tetrachloroethene discharge into a river channel through the hyporheic zone. In addition to this, Huber and Huggenberger (2016) have used GPR in a braided river (Tagliamento river, Italy) determining possible advective mixing, helping in the interpretation of ecological processes such as in the hyporheic zone. It is also worthy to highlight the use of another non-invasive technique, such as the parametric echosounder, to image the internal structure of dunes formed in the river bed (Sambrook Smith, 2013).

Riparian zone can be defined as transitional areas occurring along land and freshwater ecosystems, characterized by distinctive soil, hydrology and biotic conditions strongly influenced by the stream water (Naiman et al., 2005; Verry et al., 2000). In this study, investigations using a combination of novel in-stream GPR in conjunction with riparian surveys are applied to identify the spatial patterns and extent of low conductivity structures in the streambed and riparian zone that have been found to control groundwater – surface water exchange fluxes and residence time distributions at the interface between aquifer and river. Knowledge of the architecture and structure of fluvial deposits in such riparian and streambed zones has previously been proven to be paramount for assessing the hydrological and pollution buffering functions of riparian and hyporheic zones (Krause et al., 2011).

The main objective of the study was to verify the effectiveness of GPR imaging for sedimentological studies of river channel and floodplain drift deposits. In this study, ground-truthed GPR surveys are carried out to: (1) Characterise the sedimentary architecture of the streambed and riparian zone; (2) Identify radar facies representative of lowland meandering fluvial architectural elements observed in drift deposits; (3) Reconstruct the quasi-three-dimensional GPR profiles from closely spaced grids of two-dimensional GPR data for the subsurface floodplain sediment deposits; (4) Delineate low conductivity layers across heterogeneous streambed and riparian sediments and

(5) Discuss potential implications of identified hydrofacies for the control of groundwater-surface water exchange fluxes.

2. Materials and methods

2.1. Study area

The study area (River Tern) is a tributary of the River Severn which is located in central England, UK (Fig. 1). The investigated field site ($2^{\circ} 53'W$, $52^{\circ} 86'N$) covers an approximately 240 m long section, 4–8 m wide and extending into the extensive, predominantly agricultural floodplain on the west side of the river (Fig.1). The annual flow regime follows a stable Atlantic pattern (Arnell, 2002). Winter high flows cause channel to groundwater recharge and summer low flows are fed by groundwater discharge (Wheater et al., 2007). During prolonged periods of over abstraction and/or dry weather, river levels and water supplies are maintained by direct aquifer-to-river pumping from the underground, Permo-Triassic Sandstones (Shropshire Groundwater Scheme, Voyce, 2009). The course of the River Tern in the study area is largely natural and has not been significantly modified by human activities since the mid-19th century (Keery, 2005). The mean river discharge is $0.855 \text{ m}^3 \text{ s}^{-1}$ with a 95% exceedance (Q95) of $0.413 \text{ m}^3 \text{ s}^{-1}$ and a 10% exceedance (Q10) of $1.385 \text{ m}^3 \text{ s}^{-1}$ (data period 1972–2017, UK National River Flow Archive, <http://www.ceh.ac.uk/>). Maximum annual peak flows recorded range from $2.802 \text{ m}^3 \text{ s}^{-1}$ (January 1984) to $18.406 \text{ m}^3 \text{ s}^{-1}$ (November 2000). The river exhibits a baseflow-dominated flow regime with a high baseflow index of 0.77 (Marsh and Hannaford, 2008). Groundwater seepage from the highly permeable Permo-Triassic Sandstones maintains the high baseflow rate during dry weather periods (from May to October, Shepley and Streetley, 2007). This is reflected by the substantial 95th exceedance percentile flow of $0.653 \text{ m}^3 \text{ s}^{-1}$ which is approximately half of mean flow (Marsh and Hannaford, 2008).

Under the lowland catchment research (LOCAR) thematic programme, the investigated stream reach was selected by the UK's Natural Environment Research Council (NERC) as a typical lowland groundwater-fed river section in the UK. The field site geology along the alluvial corridor is dominated by heterogeneous alluvial drift deposits of Pleistocene to recent age forming variable thickness across the Tern catchment (Adams et al., 2003; Angermann et al., 2012). These deposits overlie the highly permeable Permo-Triassic Sherwood Sandstone (PTS) formation (Wheater and Peach, 2004), which is considered one of the regionally significant aquifers in the UK and is also

the main source of water in the Tern River (Weatherill et al., 2014). In local terms, the investigation region is based upon the Permian Bridgnorth sandstone (Fig.1), and forms the principle aquifer (Streetly and Shepley, 2005; Weatherill et al., 2014).

In the study area, the river corridor is incised, cutting through shallow, heterogeneous fluvioglacial sediments (Adams et al., 2003) which are typically composed of silt, clay, various sizes of sands, gravels as well as organic materials (Naden, 2011; Krause et al., 2012b). Floodplain core logs in the western river bank display high spatial variability in textural facies and stratification as a result of the postglacial depositional history and are characterized by a wide range of hydraulic conductivities (Krause et al., 2012b; Weatherill, 2015). Unconsolidated streambed core sediments of the high permeable layer, for instance sand and gravel, are characterised by hydraulic conductivity between 10^{-3} and 10^{-5}ms^{-1} (Angermann et al., 2012; Krause et al., 2012b). The streambed is furthermore characterized by the presence of low permeability layers such as organic peat and clay lenses (Krause et al., 2012a). Krause et al. (2012b) presented substantially lower hydraulic conductivities ranging between 10^{-8} and 10^{-9} for the clay and peat heterogeneities deposited in the streambed of the Tern River.

2.2. Ground-truthing of geophysical observations

In order to accurately interpret GPR survey data, ground truth data is imperative. Therefore, on a number of the NE-SW and NW-SE intersection lines and some distinct locations in the river channel, several bank exposures and corings from auger holes were analysed (Fig. 3). This facilitated the identification of the size and composition of alluvial deposits in the floodplain and riverbed, in addition to aiding in the determination of the interfaces of the sediments that the GPR images identify as distinct reflectors (Bridge et al., 1995; Sambrook Smith et al., 2006). Ground-truthing locations and their spatial relation to GPR transects are shown in Table 2.

Sediment coring was used to verify features present in the GPR profiles. Floodplain core sediments were retrieved using an extendable hand-driven gouge auger set (Eijkelkamp, The Netherlands) with a blade of 6.5 cm in diameter and 50 cm length (Fig. 2A). The auger was applied to characterize sediment heterogeneity in the top 170 cm to 250 cm of the floodplain. Sediment core logs were dug to the required depth using a hammer. After extraction, the cores were photographed (Fig. 2B), analysed visually and interpreted in situ.

Riverbed core sediments were retrieved using 2 m long plastic uPVC tubes (unplasticised polyvinyl chloride) (Fig. 2C). The ends of the plastic tube were sealed and large rubber bungs were used to secure the plastic sheeting. The tube was driven into the riverbed; a hammer was used where needed to facilitate digging into the riverbed. The locations of the floodplain and riverbed sediment cores are shown in Fig. 3.

Furthermore, two geological bank exposures were examined, which in turn facilitated obtaining some initial information about preserved lithology in the study section. These outcropped banks are extensive and naturally formed from collapse and erosion of the recent bank side (Fig.6).

2.3. GPR survey on floodplain and river channel sediments

Ground penetrating radar (GPR) surveys were conducted to characterize reflection patterns and delineate the type and extent of complex and spatially heterogeneous sediment facies of high and low conductive materials. Floodplain GPR surveys were conducted in August 2014 along a 240 m section of the river channel and the west bank site of River Tern, a UK lowland meandering stream. The PulseEKKO PRO radar system (Sensors and Software Inc., Canada) was used for this survey. Lightweight 250 MHz center frequency bistatic shielded square transducer (0.3 m x 0.3m in dimension) antennas have been used in this study. The antennas with an 165 pulse voltage were separated by 0.4 m and attached to a cart. These were then dragged along the floodplain profile lines, thereby generating a large number of 2-D profiles. An odometer wheel was used to trigger the measurement. The 250 MHz antenna, was chosen as compromise between the resolution and the desired penetration depth. The maximum depth range of the 250 MHz antenna in soils with high electrical conductivity like clay could reach to 2-4 m while in sandy soils it could reach to more than 10 m depth (Jol and Bristow, 2003).

In order to conduct a floodplain GPR survey of unprecedented spatial detail, 12 NE-SW and 6 NW- SE orientated transects were collected creating a raster of approximately 10 m (Fig. 3). The NE-SW orientated transects were 50 m long and ran from NE (close to the active river channel) towards SW (away from the river channel), while NW-SE transects consisted of between 100 and 132 m. The non-equal lengths in NW-SE GPR line transects were caused by the meandering of the modern river channel (Fig.3). Parameter settings during the GPR measurements for all floodplain GPR transects are shown in Table 1.

The floodplain GPR surveys were accompanied by a longitudinal in-channel GPR survey (Fig. 3) for which the antenna was deployed on a floating device. The antennas and battery were mounted on the surface water inside the bottom of plastic boat. A rope was attached to both sides of the boat to facilitate pulling. Alongside the west bank of the river, 22 ranging plastic poles were positioned with a distance of 10m separating them. The ranging poles acted as land markers to aid in the identification of distinct places alongside the river channel. The survey was conducted from the upstream to the downstream section (Fig.3) covering a length of approximately 240m of the stream.

2.4. GPR data processing

The GPR profiles were processed using the Radpro 3.2 software and involved the following processes.

- 1) Dewow: was used to remove the unwanted low-frequency noise.
- 2) Automatic gain control (AGC): AGC attempts to equalize the amplitudes of all GPR signals by applying a gain which is inversely proportional to the signal strength (Sensor and Software, 2005). In areas of weak signal, a gain is large and in areas of strong signal, the gain is small (Jol and Bristow, 2003). This type of gain is most useful for defining continuity of reflection events (Cassidy and Jol, 2009), but obliterate all amplitude information (Jol and Bristow, 2003). AGC start time zero and window size 30 ns have been used for floodplain and riverbed GPR profiles.
- 3) Band-pass (frequency domain filters): Low cut filtering (50-100 MHz) and high cut filtering (300-450 MHz) was applied to cut the unwanted noise at the low and high ends of amplitude spectrum (Best et al., 2006; Cassidy and Jol, 2009).
- 4) Time zero shift correction: was carried out to correct zero time of the first wave arrival. This correction is necessary for the accurate position of the GPR reflections on the vertical scale (Lejzerowicz et al., 2014).
- 5) Topographic Adjustment: was conducted by lowering or increasing traces, by a suitable two-way travel time (TWT), in relation to a common datum.

2.5. Radar facies identification

Characterization of the radar facies was performed according to the principles of radar stratigraphy (Beres and Haeni, 1991), which are derived from seismic stratigraphy (Mitchum et al., 1977). Radar facies refer to the sum of all the characteristics of a reflection configuration induced by a sedimentary sequence or distinct rock formation (Van Overmeeren, 1998). They are defined as mappable 2-D units, comprising reflections with an internal reflection pattern, continuity, amplitude, shape, and external 2-D form that differs from adjacent units using the approach applied by Beres and Haeni (1991), Heteren et al. (1998); Ekes and Hickin (2001).

3. Results and discussions

3.1. Ground-truthing data

The upper sections of floodplain core samples, at the northern part of the field site (C.S.1, C.S.2 and C.S.3; Fig. 3) consisted of poorly consolidated, fining upward sequences of dark brown muddy sand, containing occasional gravel and being rich in plant roots (Fig. 4). In C.S. 2, interbedded pale yellow sand with thin layers of dark grey to black silt was observed over a depth of 1 m. This layer was underlain by weathered bedrock Permo-Triassic sandstone. Through C.S.3, organic fragments and clay nodules permeate muddy sand layers between 60-90 cm in depth. In the middle part of the floodplain (C.S.4), the upper 60 cm of the core was found to be dominated by reddish brown muddy sand interbedded with sandy mud rich in organic matter in which plant roots are abundant. A similar layer was also observed in the top part of C.S.5, C.S.6, and C.S.7. Below this, a layer of saturated sand was observed from a depth of 60 to 120 cm in C.S.4. with 35 cm of grey to blue soft clay observed from a depth 120 to 155 cm. From 155 cm to approximately 200 cm the core consists of very soft black peat (Fig. 4). At the southern part of the study site (C.S.5), in particular, areas far from the active river channel, the top 80 cm was composed of unsaturated fine-grained sandy mud that was rich in organic matter and occasionally peat. Below this, more heterogeneous saturated muddy sand, rich in organic matter, peat, and clay layers with rising water levels were observed at a depth of 80 cm to 200 cm in C.S.5 during coring. Sand interbedded with silt which was observed in bank exposure 1 and C.S.2 was again observed at C.S.6 at a depth of 75 to ~ 205 cm.

In riverbed core samples, at the upstream section (e.g. R.C.1 and R.C.2; Fig. 5), the upper section was dominated by poorly sorted gravelly sand with sand sediments. A considerable

thickness of sandy clay was observed on the lower section of the core. In mid-stream sections (e.g. R.C.3 and R.C.4; Fig. 5), the top sediment was composed of a mixture of poorly sorted gravelly sand interbedded with medium-fine sand including a small organic matter fraction. The bottom sand layer has stringers of grey-to-brown organic silt. A layer of sandy or silty peat was encountered at the base of the core R.C.4, whereas in R.C.5 the competent red-to-orange Permo-Triassic sandstone was observed at the base. In the downstream section, at R.C.5 (Fig. 5), the whole 60 cm of the retrieved core was composed of fine muddy sand very rich in organic matter, a clay component and wood fragments which are present in patches. At R.C.6, a fining down succession is observed in the upper meter of the core. Gravelly sands were in the first 25 cm below the riverbed, this was found to be underlain by medium sand including stringers of grey-to-brown organic silt which was further underlain by unsaturated sandy or silty peat. Taking all this into account, a certain relationship between the core location and the lithologic variability of the river bed sediment can be seen. The core samples located upstream, both at river bend apex (R.C.1) and straight section (R.C.2) have a larger content of coarse materials, such as gravelly sand and medium to coarse sands, whereas the samples located downstream in areas before pool structure (before bend) (R.C.3-R.C.4) are predominantly composed by sand particles. (R.C.5 – R.C.7) are comprised of finer materials, such as muddy sand, silty/muddy sediment rich in organic matter and peat (Fig. 5 and 10).

In bank exposure 1, the top 75 cm of the outcrop was composed of fine to medium sand with clay fractions and organic fragments. Below this, approximately 120 cm is composed of pale yellow coarse sand interbedded with thin layers of dark grey to black silt including organic debris. This was overlain by a very thin (3 cm) layer of gravel (205-208 cm). A layer of soft black peat, approximately 12 cm thick from 208 to 220 cm, was observed to be underlain by gravel layer. From 220 to 240 cm, a clay layer was encountered at the bottom of the outcrop (Fig. 6 B). Pebbles and cobbles supported within a peaty clay matrix were encountered to a depth of approximately 160 cm of the exposure 2 (Fig. 6 A).

3.2. Radar facies identified on the west bank (floodplain) study site

Twelve NE-SW orientated GPR transects, with six intersecting NW-SE orientated transects, were collected on a west bank site of the River Tern at Heathbrook Farm (Fig.3). Individual transect interpretation are shown in appendix 1 and 2. Fig. 7 shows the overlapping cores with GPR transects as well as detailed interpretations of GPR signal patterns (radar facies). Based on distinct GPR signal reflections, eight different radar facies were identified in the study area (as illustrated in Fig.

8).

Radar facies type 1: horizontal-to-sub-horizontal reflections (Floodplain fines)

Description

This radar unit is characterized by very strong amplitudes; wavy and even horizontal-to-subhorizontal reflections with localised sparse reflections (Fig. 7, 8 and 9). This facies dominates the upper parts of all floodplain GPR transects, and with a perfect lateral continuity (Fig. 9).

Interpretation

The uppermost wavy horizontal to subhorizontal with small hyperbolic (sparse) reflections agree well with muddy sand, gravel, plant remains, clay nodules, as well as some scattered gravel (C.S. 1, 2, and 3, Fig. 5). This unit is abundant in proximal areas of the active river channel in particular in the northern part of the floodplain and can be seen up to 1.7 m depth (Fig.11). Locally, hyperbolic (sparse) reflections indicate texturally coarse grain materials (gravel) within a fine matrix element (Heteren et al., 1998). The existence of few scattered pebbles indicated that flooding of the adjacent areas was of sufficient vigour, at least initially, to deposit coarser-grade material before standing water conditions and deposition of fine-grained from settling took place (Wakefield et al., 2015).

Even-horizontal reflections are generally distinguished by the limited apparent thickness and can be seen within a depth of 0–0.75 m. This correlates with stratified muddy sand rich in organic matter and occasional peat (C.R. 4, 5, 6, and 7; Fig. 5). This feature is abundant in distal areas of the river channel, especially in the south and southwest part of the floodplain (Fig. 11). In spite of having strong dielectric contrasts between sand and peat layers, there is no distinct reflection which would mark the peat to sand interfaces in the top part of GPR profiles (e.g. line 19). The reason may be peat deposits include mineral admixtures. Sass et al. (2010) pointed out that dielectric properties of peat can be influenced by the allochthonous minerogenic material. Weatherill (2015) found low resistivity values (40–120 Ω .m) at the top part of ERT profile surveys conducted for the same region of the investigated floodplain section. Weatherill (2015) interpreted this layer as alluvial cover deposits containing a main fraction of fine-grained, conductive materials.

Generally, these reflections (horizontal-to-sub-horizontal reflections) might represent the bottom of fine-grained floodplain (overbank vertical accretion) deposits which form the youngest

stratigraphy unit in the study area. This unit of deposits formed by settling of fine-grained sediment from suspension or by flood events when the floodplain was inundated (Miall, 1996; Słowik, 2014b). The presence of minor interbedded gravel deposits indicates variations in river flow discharge and local channelized bedload transport on the river bank (Kostic and Aigner, 2007b).

Such interpretations coincide with findings of those of Asprion and Aigner (1999), Ekes and Hickin (2001) and Hickin et al. (2009) where they interpreted horizontal reflections as stratified sheet floods or vertically accreted bed-load sheets. In several of Słowik's research papers (2012a, 2012b, 2013a, 2014a) carried out for the lowland meandering Obra river in Poland, horizontal reflections were abundant in the top part of the GPR sections and were interpreted as the traces of horizontal bedding in sand deposits that might have been accumulated by a series of flood events.

A prominent alteration in GPR reflections from sigmoidal to divergent cliniform (facies 2) to horizontal (facies 1) led to the deposition of heterogeneous layers. This feature was observed clearly in south-western part of GPR line 94 (Fig. 6C and appendix 1). Possible powerful sheet-floods may have eroded the floodplain deposits (Fig. 6C). The resulting deposited horizontal sheet layers are recognized by very low and high amplitude horizontal reflections. This observed from 0 to 27 m in transect 94 (Fig. 7 A, Fig. 6C). Sheet-like deposition may have resulted in the formation of homogenous bodies of sands (Huisink, 2000).

3.2.1. Radar facies type 2: Sigmoidal to divergent cliniform reflections (modern floodplain)

Description

This radar facies is recognised by sets of sigmoidal to divergent reflections, high-to-low amplitude reflectors, slightly inclined (1° - 10°) towards the main channel river, striding onto a slightly undulatory reflector and good penetration (Figs. 6 B, 8 and 9). This facies can be seen exclusively in a few 2D profiles in NE-SW and NW-SE directions, close to the modern river channel. For example, these occurred between 27.1–48 m as multiple sets of deposition in profile 94 at a mean depth of about 0.7–3.5 m b.l.s., 2–7 m of profile 19 at a mean depth 0.7–2.5 m, 40–46 m of profile 95 at 2–3.5 m depth, 20–26 m, and 34.5–40 m of the profile 96 (see Appendix 1 and 2 for details).

Interpretation

This facies correlates well with low angle and streamward-dipping interlaminated sand with

dark grey to black silt occurring between 0.75 m and 2 m over an extensive bank exposure 1 (Figs. 4 and 8). The lower part of this reflection is characterised by low-intensity signals which attribute to the presence of clay laminae with localised concentrations of black, organic remains (Fig. 4). This unit was also observed in core sample 2 and 6 (Fig. 4) which mainly located at the head of the meander. A complicated sigmoidal reflection configuration coincides with a variety of internal structures; for example, epsilon cross stratification (ECS) and longitudinal bar foresets, which in turn are an indication of point bar deposits as well as river channel and bar migration (Ekes and Hickin, 2001). Based on these characteristics as a whole, this radar facies can be interpreted as floodplain sediments. This interpretation is supported by the fact that the GPR line 94 was surveyed in the vicinity of the modern active channel (Fig. 3).

3.2.2. Radar facies type 3: Wavy and inclined reflections (Lateral or downstream accretion elements)

Description

Radar facies 3 is characterized by variable orientation and dip of reflectors, medium-to-low amplitudes. It is bounded by a lower erosion surface and an irregular upper surface and is the most common facies in the study area and can be seen in different depths (Fig. 8).

Interpretation

This facies mark layers of sand deposits which are exhibiting fining upward sequences. This facies can be interpreted as the lateral migration of river channel (Kostic and Aigner, 2007b; Slowik, 2013a) in which indicating the development of point bars deposits (Vandenberghe and Van Overmeeren, 1999; Slowik, 2015) or may represent downstream accretion elements as well (Hickin et al. 2009). It can be seen from transect 19 (Figs. 7 and 9) at 26—39 m that the orientation of reflectors is variable, suggesting frequent changes in migration direction of the channel. A similar feature was identified by Slowik (2013a) in a study on the Odra River floodplain in Poland.

3.2.3. Radar facies type 4: Faint sub-horizontal, undular, variable dip and structureless reflections (channel-fill facies) with (abandoned channel elements)

Description

This facies is presented in GPR as a very weak amplitude, faint sub-horizontal, undular, variable dip and structureless reflection. This facies is recognized by irregular geometry that is

undulating and disturbed, with a total absence of lateral continuity (Figs. 7 and 9). This unit is bordered by horizontal reflections at the top and curved, concave up reflections at the bottom. The penetration of GPR within this unit is contingent upon the quantity of low permeability layers representing channel fill sediments. Typically, these reflectors were prevalent across the majority of the floodplain GPR profiles at variable depths.

Interpretation

This facies exhibits an important attenuation that is comprised of peat, clay and/or saturated alternate combinations of low conductivity materials (Fig. 8), evidenced by a low-energy depositional setting characterised by uneven sedimentation (Heteren et al., 1998). It is widely acknowledged that low conductivity layers can excessively attenuate GPR signals, reducing the depth of penetration (Theimer et al., 1994; Heteren et al., 1998; Bristow and Jol, 2003). Nevertheless, it can be constructive as a means of assessing the alluvial fill thickness, as observed by Leclerc and Hickin (1997) as well as Froese et al. (2005). Boisson et al. (2011) determined that heterogeneities within silt sediments produced electromagnetic energy losses of a GPR signal. However, Bristow et al. (1999) had observed that an antenna resolution that was low in respect to the sediment's internal architecture may consequently produce free GPR signal reflections. In the instance of this study, for both the floodplain and river channel GPR survey the attenuation was a consequence of the presence of low permeability layers, for example, the peat and clay deposits that were detected by the core logs (C.S. 3, 4, and 5 in Fig. 4).

C.S.5 was overlapping with the GPR transect 19 at position 90 m (Fig. 7 C). Using the lithological information, boundaries between units characterised by similar reflections were outlined. For example, saturated layers of muddy sand rich in organic matter, peat and clay (C.S. 5, Fig. 4) detected from 80 cm to 200 cm depth correlates well with this facies. This radar facies was predominantly found in the floodplain's south and southwestern areas (Fig. 11) that are characterised by low topography, particularly below facies 1 unit. This radar unit (low conductivity channel fill sediments) propagated through GPR transects 09, 10, 11, 12 and 13 in a NE-SW orientation profile, as well as lines 17, 18, 19 and 20 in a NW-SE orientation profile within the depth range of 0.8–2.5 m (Fig. 9). Furthermore, it has been observed that this facies cannot be delineated all along the profiles and it seems to laterally disappear corresponding to a body of finite length (Fig. 9). The resulting shape is similar to a lenticular body, with a flat uppermost boundary and a concave upwards bottom, which eventually tapers thinner at both of the sides approaching the

adjacent point-bar sediment deposits (Figs. 7 C and 9). Considering this characteristic, it may correlate to the infilling of an abandoned channel filled by low conductivity layers. This unit's maximum lateral extent was 66 m and can be observed in the GPR section 20 (NW-SE orientation), analogous to the direction of river flow. In addition, there are some small channels observed in north west section of the floodplain and filled by low permeability layers (GPR line 96-99) (Appendix 1). Those channels observed in GPR profiles 99,09, 10, 11, 12, 15 and 16 (Fig. 9), situated in the south-eastern region of the study area in close proximity to the hot spot section of the active channel represent chute channels. Here, the channel's internal EM signal gradually weakened with greater depth. This is likely to be a consequence of the high water level, alongside the higher electrical conductivity apparent within the clayey peat infill that contributed to significantly attenuated radar waves. This attenuation obstructed the base of the channel from being observable due to rather large thickness of low conductivity layers. Furthermore, the channel fill was also comprised of a number of small hyperbolic reflections of facies 6 at the top of the channel, which was likely to correspond to some buried boulders (Fig. 9). The filling submerged channel in the NE part of the west bank site expressed irregular reflections that were filled with stacked hyperbolic reflections (facies 6), typically associated with signal attenuation that indicates high groundwater water level. Moreover, the material infilling the channel in the central region of the floodplain (colored white in Fig. 9) displays more vigorous and continuous sub-horizontal reflections in GPR sections, while being dissimilar from infillings of the channels (green colour in Fig. 9). The almost wholly saturated sand recovered at 60–120 cm depth of floodplain core sample 4 (C.S. 4, Fig. 4), at position 10 m of GPR profile 09, corresponds largely to the features of its reflections. The location of channels colored white in Fig. 9 mainly relates to the positions of the formerly active river channel that, following its abandonment, was infilled with sand layers. Similar GPR reflections and interpretation were found in several other studies (Leclerc and Hickin, 1997; Vandenberghe and Van Overmeeren, 1999; Slowik, 2012b).

The existence of peaty channel-fill in this floodplain area may indicate either that the abandoned channel has not received clastic material over a considerable period. Consequently, this may suggest either that the active channel was not in close proximity during the infilling process or that the river bed was close, but the cutoff channel was sealed by plug bars, and there was no flood event strong enough to breach the bars and reactivate the cutoff channel. A sand layer topping may be connected to a reactivation of the depression. As abandoned channel features remain as topographical depressions in the floodplain over a considerable duration of time, running into

centuries, they are commonly disposed to channel reactivation or crevasse splay formation, both of which can explain the presence of sandy deposits close to the surface. Miall (1996) and Kostic and Aigner (2007b) stated that during the process of cut-off from the main flow, the abandoned channels were gradually packed with fine grains from suspensions.

3.2.4. Radar facies type 5: Curved, concave-upward reflections (erosional surface)

Description

This facies is characterised by high amplitude, curved, and concave upward reflections associated with dipping and small hyperbolic reflections (Fig. 8). Generally, this type of reflection is abundant in the study area and can be found below channel fill facies 4 elements (Figs. 7 C and 9). The occurrence of this configuration provides significant information concerning the previous functioning of riverbeds in the study site.

Interpretation

It should be noted that in GPR image results, this reflection is characterized by strong intensity due to the strong contrast in dielectric properties with channel fill elements of facies 4. This pattern is consistent with sand deposits rich in wood fragments which were detected at the base of the core sample 5 (C.S.5, Fig. 4). Local hyperbolic reflections mark wood fragments inside sand deposits. This unit might represent the pre-existing deposits on top of which the abandoned channel has developed. The base of the channel corresponds to an erosional surface overlaid by the sand deposits rich in wood fragments constituting the channel fill. Many studies identified similar characteristics in their study areas (see, e.g., Vandenberghe and Van Overmeeren, 1999; Lunt et al., 2004; Słowik, 2014a).

3.2.5. Radar facies type 6: Discontinuous, chaotic or irregular rich in macro scale abundant stacked hyperbolic reflections (buried boulders or bedrock surface)

Description

This facies was identified on several GPR transects (in both orientations) at a range depth 0.8–2 m, most of which were collected in areas nearby the head of the meander bend. Their stacked hyperbolas reflections resemble inverted chevron shapes (Fig. 7).

Interpretation

Hyperbolic reflections appear as a consequence of the response of the divergent radar beam to extremely uneven boundary (Heteren et al., 1998). The antenna receiver obtaining electromagnetic waves not only via reflection on the near-horizontal boundary but also via reflection of that part of the peripheral GPR beam that forms a fresnel zone on subhorizontal to sharply inclined boundary surfaces (Heteren et al., 1998). When compared bank exposure 2 (Fig. 6) to the GPR profile 94 (position 6 to 20 m), at the range depth 0.5–1 m, different gravel sizes supported within a peaty sandy clay matrix could match this facies. This can be considered as a part of paleo-meander channel fill sediments. Another interpretation could be representing the top of the irregular surface of Permo-Triassic sandstone bedrock (C.S.2, Fig. 4).

3.2.6. Radar facies type 7: High amplitude, discontinuous hummocky and chaotic reflections including micro-scale hyperbolic diffractions (alluvial deposits with pebbles).

Description

Facies 7 is observed in most of the NE-SW and NW-SE oriented GPR 2D profiles within the depth range 0.7-2 m, observed around channel fill elements (Fig. 7).

Interpretation

Unfortunately, there is no ground truth data for validating this facies. This unit exhibits several small-scale hyperbolic diffractions which should correspond to point objects buried at different depths, probably being large clasts (e.g. small boulders) within sand deposits. Moreover, their geometry fit well with 0.08-0.1 m/ns electromagnetic (EM) velocity value.

These configurations suggest the existence of a heterogeneous lithological unit of high conductive materials which surround older channels and indicate sediments of bar deposits. This facies was also present in Zuk (2011).

Radar facies type 8: Structureless, reflection free zone

Description

This facies can be identified in the middle part of the floodplain section, specifically in the area of low topography close to the second meander bend. They have been imaged in both NE-SW profiles (profile 99 and 09) and NW-SE profiles (profiles 16, 17, and 18), below subhorizontal reflection patterns of sandy channel fill deposits (Fig. 9).

Interpretation

Structureless facies may indicate the presence of large thickness highly conductive materials (Ekes and Hickin, 2001). In the study site, this facies seems to disappear laterally in both GPR direction profiles, corresponding to a body of finite length (Fig. 7 C and 8). These structureless signals correlate well with the retrieved clay layer (~ 35 cm thick) observed at a depth of ~ 120 cm, extending up to 155 cm in depth in core sample 4 (Fig. 4). Clay has dramatically attenuated the GPR signal, because it is comprised of charged particles.

3.3. Longitudinal streambed GPR survey

Description

The longitudinal GPR survey was performed to investigate the detailed internal structure of streambed deposits. It revealed geomorphological features that included former channel fills and the lateral accretion of point bars (Fig 10). However, horizontal, wavy, dipped, curved, concave-up, attenuation, and multiple reflections can all be discerned in the GPR image. The first strong undulating reflection represents the bottom of the river (the sediment-water interface), providing useful bathymetry observations. Subsequent reflections are from the sediment structure on the sub-bottom of the river. The strong reflection obtained from the bottom also produced some multiples (Fig. 10). The signal reflected from the bottom, traveled up to the surface, was reflected from the water-air interface and then traveled back down to be reflected from the bottom a second time before traveling again to the surface. Such results are easily interpreted, because they take double the travel time of a bottom only reflector. The clearest example is visible between 140 m and 190 m.

The first ~ 57 m of the river profile correspond to the E-W orientated section of the river, and the upper reflections from the top 20 to 50 cm of the riverbed are characterized by high and low amplitude sub-horizontal signals, associated with chaotic and disturbed reflections. Below this level, there are a set of dipping reflections, associated with low amplitude disturbed reflections from ~ 17 m to ~ 30 m, which reveal greater thickness than in other regions. These reflections correlate with sandy silt that is rich in deposits of organic matter, and the dipping reflections can be interpreted as constituting lateral accretion.

The river makes a right turn towards the south at about 60 m along the profile, after which

point, water flows South, until 200 m of the transect. The uplift area observed between 57m and 62 m represents the inner bank of the meander. It is composed of fining-upward sequences of point bar deposits of gravely sand and muddy sand sediments (R.C.1, Fig. 5). From ~ 62 m to ~ 98m of the longitudinal profile, different GPR signal reflections were identified, for example, dipping, subhorizontal and dipping reflections, which may represent sediments created by the erosion of the cutbank. In the radargram, the reflections arise from high amplitude reflectors, which correspond with the highly permeable sand and gravel deposits identified in core samples 2–4 (Fig. 5). A lens of sandy clay layer was identified at 77 m–88 m, at a range depth of 40–80 cm, and recognised by a trough-shaped reflection in the GPR image (Fig. 10). This finding was confirmed during the installation of minipiezometers in the riverbed.

At ~ 100 m to ~130 m along the profile, the upper reflections are characterized by medium to strong subhorizontal reflectors, which are associated with small hyperbolic reflections, with good lateral continuity. These reflections indicate high permeability layers such as gravel and sand with minimal organic matter content, in accordance with the river core sample 1 (R.C.3, R.C.4, Fig. 5). Below this level, the GPR result shows signal attenuation is associated with disturbed and weak amplitude, and wavy to sub-horizontal reflections. The underlying reflections correlate with the sandy or silty peat layers identified at the bottom of the core sample (R.C.3). It has been noted that from 125 m to ~ 135 m of the profile the signal shows a lens comprising disturbed and attenuated features, which might denote sediments rich in organic matter or peat. The longitudinal GPR survey result covering this section (~ 98 m to ~130 m) reveals the predominant high permeability layers in this region have a greater thickness comparative to the other parts of the profile (Fig. 10). Regarding the geological characteristics, R.C.3 and RC.4 were retrieved at positions 100 m and 125 m of the GPR profile respectively. An ERT survey for this section by (Naden, 2011), found high resistivity values in the subchannel section, which was interpreted as layers of superficial sand and diamict deposits.

The area 140 m to ~ 192 m along the profile is characterized by low surface water level (Fig. 10). Geophysically, the first strong reflections were diagnosed by disturbed subhorizontal reflections. This agrees well with the presence of a gravely sand top unit rich in organic matter, as identified in riverbed core samples 5-7 (Fig. 5). Below this, the area is characterized by a strong GPR signal, including disturbed and attenuated alternates showing multiple reflections from surface water (Fig. 10). This is corresponding with peat and clay layers identified in riverbed core samples

5-7. This area is corresponding with south east section of the floodplain which also was rich in low permeability layers. Previously, Krause et al. (2012b) also identified these layers in this section. The presence of subchannel low conductivity layers, such as clay, peat, and sediments rich in organic matter content resulted in GPR free signal reflections, due to the absorption of the majority of the electromagnetic waves (Davis and Annan, 1989). In this study, GPR was able to delineate the spatial extent of low conductivity structures in the riverbed which we never had evidence for their spatial extent.

Interpretation

Concave-up reflections can be associated to the presence of an erosional surface related to channel bottom. They can be overlaid by both dipping reflections (e.g. the reflections from ~ 17 m to ~ 30 m) and wavy and subhorizontal reflections (e.g. the reflections from ~ 110 m to ~ 130 m). In the first case, dipping reflections are associated to prograding channel bars constituted by sand interbed with silt and rich organic matter, indicating traces of growth of the barforms at high flows (e.g. Slowik, 2018). In the second case, wavy and subhorizontal attenuated reflections correspond to sandy and silty peat deposits (as observed in the bottom of R.C.3 and R.C.4 core samples) representing the infilling of a previous channel due to a decrease of the energy and capacity transport.

3.4. Permeability class distribution

Fig. 9 shows the permeability class distribution in the west bank river site (riparian zone, outlined in green). The results of quasi three-dimensional GPR images (Fig. 9) revealed that the low permeability layers are distributed in different places with various thicknesses and extensions. The distribution of clay and peat layers (low conductivity layers) in riparian and streambed environment are responsible for the attenuation of groundwater reactive pollutants. In contrast, high conductive lithologies in that environments are found to ensure the rapid discharge of groundwater and thus give less opportunity for contaminant biotransformations. Block diagrams were created using Rockwork software (version15). Types of geologic and numeric data were represented in interpolated block diagram such as lithology distribution, stratigraphic layers, geophysical data and colours. Geophysical data was entered at depth points with optional dates. A three-dimensional geological block diagram for floodplain deposits showed that the northern part of the floodplain is rich in high permeable materials with some patches of low permeability materials (Fig. 11), whereas it is clear that the low permeability deposits are abundant in the south and southwestern part of the

floodplain. The top units of floodplain deposits are composed of muddy sand with peat. Below this, the alluvial aquitard (peat and clay) is laterally continuous representing channel fill sediments (Facies 4) (Fig. 11). The resulting shape of low permeability structures is similar to a lenticular body, with a flat top boundary and a concave upward bottom. Taking this into account, it would correspond to part of the infilling of an abandoned channel filled by peat and clay. The mapped low permeability deposits (e.g. clay and peat) (Figs. 8 and 11), which are observed on the south-eastern part of the bank, near the river, between GPR profiles 9-12, coincide with attenuated section of the river channel GPR profile (140-192 m). This is likely to be the riverward extension of low permeability layers underlying the floodplain across the active river channel (Fig. 9). The highly permeable materials in the northern part of the west bank river site correspond to non-attenuated area of river channel survey. Hence, three-dimensional geological model helped to better our understanding of the spatial variability and sediment heterogeneity in the study area.

3.5. Implications for groundwater – surface water exchange flow

Knowledge of the sedimentary structure of the glaciofluvial deposits and their internal heterogeneities facilitate a better understanding of groundwater flow and transportation of groundwater resident contaminants (Huggenberger, 1993; Kostic and Aigner, 2007b). Hydraulic characteristics are strongly controlled by sediment texture and grain size distribution. Individual lithofacies can create interconnected, hydrogeological related regions that display relatively homogeneous hydraulic characteristics defining discrete hydrostratigraphic and hydrofacies units (Poeter and Gaylord, 1990; Heinz and Aigner, 2003; Kostic et al., 2005).

Generally, various sizes of the sedimentary units in the streambed and riparian zones may form a complex three-dimensional mosaic which is thought to induce complex subsurface flow patterns (Naegeli et al., 1996). The sediment grain size influences subsurface flow paths (Steel and Thompson, 1983) which in turn affects oxygen transformation, dissolved organic carbon and the cycling of nutrients.

From a hydrogeological viewpoint, in the riparian zone of the investigated field site, the components concerned with lateral accretion elements form extensive but heterogeneous elements that are essential in the composition of the hydraulic system (Kostic and Aigner, 2007b). Such components are typified by a highly conductive, sheet-like geometry with slightly dipping layers. Characteristic interfingering occurring within variable dip lateral accretions implies that a complex

general flow system exists. This system is generally determined by the orientation of dipping, highly permeable layers (Kostic and Aigner, 2007b). However, the presence of highly conductive elements of point bar lateral accretion, shallow bedrock depth in this area, as well as high amplitude irregular reflections associated with stacking hyperbolic structures of different gravel sizes, creates good floodplain-to-subchannel hydraulic continuity in the north-eastern subsurface of the field site. The sub-channel region associated with this part of the floodplain is made up of shallow sand and diamictic layers. These layers exhibit a fairly high degree of hydraulic conductivity (Krause et al., 2012), which in turn allows for the reasonably rapid discharge of groundwater into the river channel. The residence time of water would be therefore low in this section.

The low topographical area in the south and south-western part of the floodplain, low permeability dominated layers representing channel fill elements, plays a pivotal role on the hydrology of fluvial system as their presence influences the groundwater flow patterns. These sediments are also considered to be part of the drift deposits that caps the Permo-Triassic sandstone at the study area and characterized by low resistivity values, as well as very low hydraulic conductivity (Ks) magnitude (e.g., $< 0.005 \text{ md}^{-1}$) as identified by Weatherill (2015). The presence of high amounts of shallow peat and clay layers representative of channel fill deposits can control the location of the water table (Gómez-Ortiz et al., 2010). It is worthwhile to mention that the core log that exist within this channel-fill deposit unit (for example, C.S.5) correspond with the lowest hydraulic head area in the floodplain groundwater system (Fig. 12). This head pattern, which this log intercepts, can potentially be construed through a hydraulic isolation of the groundwater by the in-fill deposits produced by the regional upwelling pressure from the bedrock system in other places in the floodplain (Fig. 12).

Channels can be buried by vertical overbank deposits producing “paleochannels” where coarse particle riverbed alluvium is buried underneath fine grain floodplain deposits (Stanford and Ward, 1993). In case the water table is intercepted by the paleochannels, the paleochannels effectively act as large preferential-flow conduits capable of directing water the entire distance of a floodplain (Wondzell and Gooseff, 2013).

4. Conclusions

The local sedimentological structures preserved at the studied reach of the River Tern are were found to be highly complex and heterogeneous at very small-scales (e.g. centimetre). Hence,

quasi three-dimensional geological reconstruction of the lowland river section was undertaken to better understand the spatial distribution of sediment heterogeneity of the fluvial environments. This study demonstrates that GPR, in conjunction with robust ground truthing data, provides novel information on the sediment stratigraphy and the geometry of the sediment texture in fluvio-glacial deposits in a lowland meandering river. We therefore recommend this method for structural and lithological studies of deposits in an alluvial valley fills, for example, the hyporheic zone and the adjacent floodplain, due to the relatively high spatial resolution and the possibility to image large areas.

Eight major radar facies were recognized in the west bank of the river. Radar facies 4 and 8 marked low conductivity layers in the study area which represents channel fill sediment deposits. Lenses of clay and peat (channel fill sediments) structures were delineated in the study area based on the GPR signal attenuation in relation to the adjacent area. These structures are predominantly deposits in the south and south-eastern part of the floodplain and distributed laterally with different thicknesses and extensions. GPR survey in riverbed shows the spatial extent of low conductivity structures in riverbed determined by attenuation of signals. Spatially detailed understanding of such structures is highly valuable since sedimentary units of different grain size have been shown to create a complex pattern of subsurface flow paths. Moreover, the distribution of low conductivity layers controls the geometry and location of a local water table.

Acknowledgments

I wish to express gratitude to higher committee for education development in Iraq (HCED) who provided the funding to make this research possible. We also thank Kevin Voyce (Environment Agency of England and Wales) for providing previous data and scientific report. I would like to thank Prof. Nigel Cassidy and Dr. Jamie Pringle for training provided through the NERC geophysical skills course at Keele University. We are very grateful to the land owners at Helshaw Grange and Heathbrook Farm for permitting access to the River Tern field site.

References

- ADAMS, B., PEACH, D. & BLOOMFIELD, J. 2003. The LOCAR hydrogeological infrastructure in the tern catchment. Groundwater Systems and Water Quality Programme, Internal Report IR/03/180. British Geological Survey, Keyworth.
- ANGERMANN, L., KRAUSE, S. & LEWANDOWSKI, J. 2012. Application of heat pulse injections for investigating shallow hyporheic flow in a lowland river. *Water Resources Research*, 48, W00P02, DOI: 10.1029/2012WR012564.
- ARNELL, N. 2002. Hydrology and Global Environmental Change. Pearson Education Limited, Essex, UK.
- ASPRION, U. & AIGNER, T. 1999. Towards realistic aquifer models: three-dimensional georadar surveys of Quaternary gravel deltas (Singen Basin, SW Germany). *Sedimentary Geology*, 129, 281-297.
- ASHWORTH, P.J., SAMBROOK SMITH, G.H., BEST, J.L., BRIDGE, J.S., LANE, S.N., LUNT, I.A., REESINK, A.J.H., SIMPSON, C.J., THOMAS, R.E. 2011. Evolution and sedimentology of a channel fill in the sandy braided South Saskatchewan River and its comparison to the deposits of an adjacent compound bar. *Sedimentology*, 58, 1860-1883.
- BERES, M., GREEN, A., HUGGENBERGER, P. & HORSTMAYER, H. 1995. Mapping the architecture of glaciofluvial sediments with three-dimensional georadar. *Geology*, 23, 1087.
- BERES, M. & HAENI, F. 1991. Application of ground-penetrating-radar methods in Hydrogeologie Studies. *Ground Water*, 29, 375-386.
- BERSEZIO, R., GIUDICI, M. & MELE, M. 2007. Combining sedimentological and geophysical data for high-resolution 3-D mapping of fluvial architectural elements in the Quaternary Po plain (Italy). *Sedimentary Geology*, 202, 230-248.
- BEST, J., WOODWARD, J., ASHWORTH, P., SMITH, G. S. & SIMPSON, C. 2006. Bar-top hollows: A new element in the architecture of sandy braided rivers. *Sedimentary Geology*, 190, 241-255.
- BINLEY, A., HUBBARD, S. S., HUISMAN, J. A., REVIL, A., ROBINSON, D. A., SINGHA, K. & SLATER, L. D. 2015. The emergence of hydrogeophysics for improved understanding of subsurface processes over multiple scales. *Water Resources Research*, 51, 3837-3866.
- BINLEY, A., ULLAH, S., HEATHWAITE, A. L., HEPPELL, C., BYRNE, P., LANSDOWN, K., TRIMMER, M. & ZHANG, H. 2013. Revealing the spatial variability of water fluxes at the groundwater-surface water interface. *Water Resources Research*, 49, 3978-3992.
- BINLEY, A., WINSHIP, P., POKAR, M. & WEST, J., 2001. Cross borehole radar and resistivity tomography: a comparison of techniques in unsaturated sandstone. In Symp. Applications of Geophysics to Engineering and Environmental Problems (SAGEEP).
- BOISSON, J., HEGGY, E., CLIFFORD, S. M., YOSHIKAWA, K., ANGLADE, A. & LOGNONNÉ, P. 2011. Radar sounding of temperate permafrost in Alaska: Analogy to the Martian midlatitude to high-latitude ice-rich terrains. *Journal of Geophysical Research: Planets*, 116, E11003, doi:10.1029/2010JE003768.
- BRIDGE, J. S., ALEXANDER, J., COLLIER, R. E., GAWTHORPE, R. L. & JARVIS, J. 1995. Ground-penetrating radar and coring used to study the large-scale structure of point-bar deposits in three dimensions. *Sedimentology*, 42, 839-852.
- BRISTOW, C., SKELLY, R. & ETHRIDGE, F. 1999. Crevasse splays from the rapidly aggrading, sand-bed, braided Niobrara River, Nebraska: effect of base-level rise. *Sedimentology*, 46, 1029-1048.
- BRISTOW, C. S. & JOL, H. M. 2003. An introduction to ground penetrating radar (GPR) in sediments. *Geological Society, London, Special Publications*, 211, 1-7.
- CARDENAS, M. B. & JIANG, X. W. 2010. Groundwater flow, transport, and residence times through topography-driven basins with exponentially decreasing permeability and porosity. *Water Resources Research*, 46, DOI: 10.1029/2010WR009370.
- CASSIDY, N. J. & JOL, H. 2009. Ground penetrating radar data processing, modelling and analysis. In: Jol, H.M. (ed.), *Ground penetrating radar: theory and application*, Elsevier: Amsterdam; 141-176.
- CLIFFORD, J. & BINLEY, A. 2010. Geophysical characterization of riverbed hydrostratigraphy using electrical resistance tomography. *Near Surface Geophysics*, 8, 493-501.
- CONANT, B. 2004. Delineating and quantifying ground water discharge zones using streambed

- temperatures. *Ground Water*, 42, 243-257.
- CONANT, B., CHERRY, J. A. & GILLHAM, R. W. 2004. A PCE groundwater plume discharging to a river: influence of the streambed and near-river zone on contaminant distributions. *Journal of Contaminant Hydrology*, 73, 249-279.
- CROOK, N., BINLEY, A., KNIGHT, R., ROBINSON, D., ZARNETSKE, J. & HAGGERTY, R. 2008. Electrical resistivity imaging of the architecture of substream sediments. *Water Resources Research*, 44, 1-11.
- FLECKENSTEIN, J. H., NISWONGER, R. G. & FOGG, G. E. 2006. River-aquifer interactions, geologic heterogeneity, and low-flow management. *Ground water*, 44, 837-852.
- GÓMEZ-ORTIZ, D., MARTÍN-CRESPO, T., MARTÍN-VELÁZQUEZ, S., MARTÍNEZ-PAGÁN, P., HIGUERAS, H. & MANZANO, M. 2010. Application of ground penetrating radar (GPR) to delineate clay layers in wetlands. A case study in the Soto Grande and Soto Chico watercourses, Doñana (SW Spain). *Journal of Applied Geophysics*, 72, 107-113.
- GOMEZ-VELEZ, J. D., KRAUSE, S. & WILSON, J. L. 2014. Effect of low-permeability layers on spatial patterns of hyporheic exchange and groundwater upwelling. *Water Resources Research*, 50, 5196-5215.
- GOURRY, J.-C., VERMEERSCH, F., GARCIN, M. & GIOT, D. 2003. Contribution of geophysics to the study of alluvial deposits: a case study in the Val d'Avaray area of the River Loire, France. *Journal of Applied Geophysics*, 54, 35-49.
- DAILY, W. & RAMIREZ, A. L. 2000. Electrical imaging of engineered hydraulic barriers. *Geophysics*, 65, 83-94.
- DAVIS, J. & ANNAN, A. 1989. Ground penetrating radar for high-resolution mapping of soil and rock stratigraphy. *Geophysical Prospecting*, 37, 531-551.
- EKES, C. & HICKIN, E. J. 2001. Ground penetrating radar facies of the paraglacial Cheekye Fan, southwestern British Columbia, Canada. *Sedimentary Geology*, 143, 199-217.
- FLECKENSTEIN, J. H., NISWONGER, R. G. & FOGG, G. E. 2006. River-aquifer interactions, geologic heterogeneity, and low-flow management. *Ground water*, 44, 837-852.
- FROESE, D. G., SMITH, D. G. & CLEMENT, D. T. 2005. Characterizing large river history with shallow geophysics: Middle Yukon River, Yukon Territory and Alaska. *Geomorphology*, 67, 391-406.
- HEINZ, J. & AIGNER, T. 2003. Three-dimensional GPR analysis of various Quaternary gravel-bed braided river deposits (southwestern Germany). *Geological Society, London, Special Publications*, 211, 99-110.
- HETEREN, S. V., FITZGERALD, D. M., MCKINLAY, P. A. & BUYNEVICH, I. V. 1998. Radar facies of paraglacial barrier systems: coastal New England, USA. *Sedimentology*, 45, 181-200.
- HICKIN, A.S., Kerr, B., BARCHYN, T.E. and PAULEN, R.C., 2009. Using ground-penetrating radar and capacitively coupled resistivity to investigate 3-D fluvial architecture and grain-size distribution of a gravel floodplain in northeast British Columbia, Canada. *Journal of Sedimentary Research*, 79, 457-477.
- HUGGENBERGER, P. 1993. Radar facies: recognition of facies patterns and heterogeneities within Pleistocene Rhine gravels, NE Switzerland. *Geological Society, London, Special Publications*, 75, 163-176.
- HUBER, E. & HUGGENBERGER, P. 2016. Subsurface flow mixing in coarse, braided river deposits. *Hydrology and Earth System Sciences*, 20, 2035-2046,
- HUISINK, M. 2000. Changing river styles in response to Weichselian climate changes in the Vecht valley, eastern Netherlands. *Sedimentary Geology*, 133, 115-134.
- JOL, H. M. & BRISTOW, C. S. 2003. GPR in sediments: advice on data collection, basic processing and interpretation, a good practice guide. *Geological Society, London, Special Publications*, 211, 9-27.
- KEERY, J. 2005. *Quantifying vertical water fluxes between groundwater and a lowland river, using temperature time series*. MSc thesis, Lancaster Environment Centre, Lancaster University.
- KOSTIC, B. & AIGNER, T. 2007a. Sedimentary architecture and 3D ground-penetrating radar analysis of gravelly meandering river deposits (Neckar Valley, SW Germany). *Sedimentology*, 54, 789-808.
- KOSTIC, B. & AIGNER, T. 2007b. Sedimentary architecture and 3D ground-penetrating radar analysis of gravelly meandering river deposits (Neckar Valley, SW Germany). *Sedimentology*, 54, 789-808.

- KOSTIC, B., BECHT, A. & AIGNER, T. 2005. 3-D sedimentary architecture of a Quaternary gravel delta (SW-Germany): Implications for hydrostratigraphy. *Sedimentary Geology*, 181, 147-171.
- KRAUSE, S., BLUME, T. & CASSIDY, N. 2012a. Application of fibre-optic DTS to identify streambed controls on aquifer-river exchange fluxes in lowland rivers. *Hydrol. Earth Syst. Sci.*, 16, 1775-1792.
- KRAUSE, S., BLUME, T. & CASSIDY, N. J. 2012b. Investigating patterns and controls of groundwater upwelling in a lowland river by combining Fibre-optic Distributed Temperature Sensing with observations of vertical hydraulic gradients. *Hydrology and Earth System Sciences*, 16, 1775-1792.
- KRAUSE, S., HEATHWAITE, L., BINLEY, A. & KEENAN, P. 2009b. Nitrate concentration changes at the groundwater-surface water interface of a small Cumbrian river. *Hydrological Processes*, 23, 2195-2211.
- KRAUSE, S., TECKLENBURG, C., MUNZ, M. & NADEN, E. 2013. Streambed nitrogen cycling beyond the hyporheic zone: Flow controls on horizontal patterns and depth distribution of nitrate and dissolved oxygen in the upwelling groundwater of a lowland river. *Journal of Geophysical Research: Biogeosciences*, 118, 54-67.
- LECLERC, R. F. & HICKIN, E. J. 1997. The internal structure of scrolled floodplain deposits based on ground-penetrating radar, North Thompson River, British Columbia. *Geomorphology*, 21, 17-38.
- LEJZEROWICZ, A., KOWALCZYK, S. & WYSOCKA, A. 2014. The usefulness of ground-penetrating radar images for the research of a large sand-bed braided river: case study from the Vistula River (central Poland). *Geologos*, 20, 35-47.
- LUNT, I., BRIDGE, J. & TYE, R. 2004. A quantitative, three-dimensional depositional model of gravelly braided rivers. *Sedimentology*, 51, 377-414.
- MARSH, T. J. & HANNAFORD, J. 2008. *UK Hydrometric Register – Hydrological data UK series*. Centre for Ecology and Hydrology, Wallingford, UK.
- MIALL, A. 1996. *Sedimentary facies, basin analysis, and petroleum geology*. Springer-Verlag, 582 pp.
- MITCHUM, R., VAIL, P. & SANGREE, J. 1977. Stratigraphic interpretation of seismic reflection patterns in depositional sequences. In: Payton, C.E. (Ed.), *Seismic Stratigraphy—Applications to Hydrocarbon Exploration*. AAPG Mem. 16, 117– 123.
- NADEN, E. 2011. *Characterisation of aquifer-to-river connectivity using hydrogeophysical methods for surface water protection*. Unpublished MSc. thesis, Keele University.
- NAEGELI, M. W., HUGGENBERGER, P. & UEHLINGER, U. 1996. Ground penetrating radar for assessing sediment structures in the hyporheic zone of a prealpine river. *Journal of the North American Benthological Society*, 15, 353-366.
- NAIMAN, R., DECAMPS, H., MCCLAIN, M. 2005. *Riparia - Ecology, Conservation, and Management of Streamside Communities*. Academic Press, 448 pp. ISBN 9780126633153.
- NARANJO, R. C., NISWONGER, R. G., STONE, M., DAVIS, C. & MCKAY, A. 2012. The use of multiobjective calibration and regional sensitivity analysis in simulating hyporheic exchange, *Water Resource Research*, 48, W01538, doi:10.1029/2011WR011179.
- NEAL, A. 2004. Ground-penetrating radar and its use in sedimentology: principles, problems and progress. *Earth-Science Reviews*, 66, 261-330.
- POETER, E. & GAYLORD, D. R. 1990. Influence of aquifer heterogeneity on contaminant transport at the Hanford Site. *Ground Water*, 28, 900-909.
- REESINK, A.H.J., ASHWORTH, P.J., SAMBROOK SMITH, G.H., BEST, J.L., PARSONS, D.R., AMSLER, M.L., HARDY, R.J., LANE, S.N., NICOLAS, A.P., ORFEO, O., SANDBACH, S.D., SIMPSON, C.J., SZUPIANY, R.N. 2014. Scales and causes of heterogeneity in bars in a large multi-channel river: Rio Parana, Argentina. *Sedimentology*, 61, 1055-1085.
- REYNOLDS, J. M. 2011. *An introduction to applied and environmental geophysics*. John Wiley & Sons, 710 pp.
- SALEHIN, M., PACKMAN, A. I. & PARADIS, M. 2004. Hyporheic exchange with heterogeneous streambeds: Laboratory experiments and modeling. *Water Resources Research*, 40, W11504, doi:10.1029/2003WR002567.
- SAMBROOK SMITH, G. H., ASHWORTH, P. J., BEST, J. L., WOODWARD, J. & SIMPSON, C. J. 2006. The sedimentology and alluvial architecture of the sandy braided South Saskatchewan River, Canada. *Sedimentology*, 53, 413-434.

- SAMBROOK SMITH, G. 2013. Decimeter-scale in situ mapping of modern cross-bedded dune deposits using parametric echo sounding: A new method for linking river processes and their deposits. *Geophysical Research Letters*, 40, 3883-3887.
- SASS, O., FRIEDMANN, A., HASELWANTER, G. & WETZEL, K.-F. 2010. Investigating thickness and internal structure of alpine mires using conventional and geophysical techniques. *Catena*, 80, 195-203.
- SENSORS AND SOFTWARE. 1996. Technical Manual 21: PulseEKKO Basic Plotting and Editing. Sensors and Software.
- SENSORS AND SOFTWARE. 2005. PulseEKKO PRO User's Guide. Sensors and Software, Ontario.
- SHEPLEY, M. & STREETLY, M. 2007. The estimation of 'natural' summer outflows from the Permo-Triassic Sandstone aquifer, UK. *Quarterly Journal of Engineering Geology and Hydrogeology*, 40, 213-227.
- SKELLY, R.L., BRISTOW, C.H.S., ETHRIDGE, F.G. 2003. Architecture of channel-belt deposits in an aggrading shallow sandbed braided river: the lower Niobrara river, northeast Nebraska. *Sedimentary Geology*, 158, 249-270.
- SŁOWIK, M. 2012a. Changes of river bed pattern of a lowland river: effect of natural processes or anthropogenic intervention? *Geografiska Annaler: Series A, Physical Geography*, 94, 301-320.
- SŁOWIK, M. 2012b. Influence of measurement conditions on depth range and resolution of GPR images: The example of lowland valley alluvial fill (the Obra River, Poland). *Journal of Applied Geophysics*, 85, 1-14.
- SŁOWIK, M. 2013a. GPR and aerial imageries to identify the recent historical course of the Obra River and spatial extent of Obrzańskie Lake, altered by hydro-technical works. *Environmental Earth Sciences*, 70, 1277-1295.
- SŁOWIK, M. 2013b. Transformation of a lowland river from a meandering and multi-channel pattern into an artificial canal: retracing a path of river channel changes (the Middle Obra River, W Poland). *Regional Environmental Change*, 13, 1287-1299.
- SŁOWIK, M. 2014a. Analysis of fluvial, lacustrine and anthropogenic landforms by means of ground-penetrating radar (GPR): field experiment. *Near Surface Geophysics*, 12, 777-791.
- SŁOWIK, M. 2014b. Holocene evolution of meander bends in lowland river valley formed in complex geological conditions (the Obra River, Poland). *Geografiska Annaler: Series A, Physical Geography*, 96, 61-81.
- SŁOWIK, M. 2015. The influence of meander bend evolution on the formation of multiple cutoffs: findings inferred from floodplain architecture and bend geometry. *Earth Surface Processes and Landforms*, 41, 626-641.
- SŁOWIK, M., 2018. The formation of an anabranching planform in a sandy floodplain by increased flows and sediment load. *Earth Surface Processes and Landforms*, 43, 623-638.
- STEEL, R. & THOMPSON, D. 1983. Structures and textures in Triassic braided stream conglomerates ('Bunter' pebble beds) in the Sherwood Sandstone Group, North Staffordshire, England. *Sedimentology*, 30, 341-367.
- STREETLY, M. & SHEPLEY, M. 2005. Final Report, East Shropshire Permo-Triassic Sandstone Groundwater Modelling Project – Task 8. Environment Agency, Bristol.
- THEIMER, B. D., NOBES, D. C. & WARNER, B. G. 1994. A study of the geoelectrical properties of peatlands and their influence on ground-penetrating radar surveying. *Geophysical prospecting*, 42, 179-209.
- TONINA, D. & BUFFINGTON, J. M. 2009. Hyporheic exchange in mountain rivers I: Mechanics and environmental effects. *Geography Compass*, 3, 1063-1086.
- TOPP, G. C., DAVIS, J. & ANNAN, A. P. 1980. Electromagnetic determination of soil water content: Measurements in coaxial transmission lines. *Water Resources Research*, 16, 574-582.
- TRAUTH, N., FLECKENSTEIN, J.H., 2017. Single discharge events increase reactive efficiency of the hyporheic zone. *Water Resources Research*, 53(1), 779-798.
- VAN DAM, R.L., SCHLAGER, W., 2000. Identifying causes of ground-penetrating radar reflections using time-domain reflectometry and sedimentological analyses. *Sedimentology*, 47, 435-449.
- VAN OVERMEEREN, R. 1998. Radar facies of unconsolidated sediments in The Netherlands: A radar

- stratigraphy interpretation method for hydrogeology. *Journal of Applied Geophysics*, 40, 1-18.
- VANDENBERGHE, J. & VAN OVERMEEREN, R. 1999. Ground penetrating radar images of selected fluvial deposits in the Netherlands. *Sedimentary Geology*, 128, 245-270.
- VERRY, E.S., DOLLOFF, C.A., MANNING, M.E. 2004. Riparian ecotone: A functional definition and delineation for resource assessment. *Water, Air, and Soil Pollution: Focus*, 4 (1), 67-94.
- VOYCE, K.J. (2009). Groundwater Management: the Shropshire Groundwater Scheme. *Proceedings of the Shropshire Geological Society*, 14, 20-29.
- WAKEFIELD, O. J., HOUGH, E. & PEATFIELD, A. W. 2015. Architectural analysis of a Triassic fluvial system: the Sherwood Sandstone of the East Midlands Shelf, UK. *Sedimentary Geology*, 327, 1-13.
- WEATHERILL, J. 2015. *Investigating the natural attenuation and fate of a trichloroethene plume at the groundwater-surface water interface of a UK lowland river*, Unpublished PhD thesis, Keele University.
- WEATHERILL, J., KRAUSE, S., VOYCE, K., DRIJFHOUT, F., LEVY, A. & CASSIDY, N. 2014. Nested monitoring approaches to delineate groundwater trichloroethene discharge to a UK lowland stream at multiple spatial scales. *Journal of Contaminant Hydrology*, 158, 38-54.
- WHEATER, H. S. & PEACH, D. 2004. Developing interdisciplinary science for integrated catchment management: the UK lowland catchment research (LOCAR) programme. *International Journal of Water Resources Development*, 20, 369-385.
- WHEATER, H.S., PEACH, D. AND BINLEY, A. 2007. Characterizing groundwater dominated lowland catchments: the UK Lowland Catchment Research Programme (LOCAR). *Hydrology and Earth System Sciences*, 11, (1), 108-124.
- WONDZELL, S. M. & GOOSEFF, M. N. 2013. Geomorphic controls on hyporheic exchange across scales: watersheds to particles. In: SHRODER, J. E. I. C. & WOHL, E. E. (eds.) *Treatise on Geomorphology*. San Diego, CA, USA: Academic Press, 203-218.
- ZUK, T. 2011. *Acquisition, 3-D display and interpretation of GPR data in fluvial sedimentology*. M.Phil. thesis, University of Birmingham.

Figure Captions

Fig. 1: (A) Overview of floodplain and river channel investigation area (GetMapping Plc; copyright). (B) Regional geology and location of the study area at the River Tern, UK. Contours of hydraulic heads based on mean monthly groundwater levels measured at Environment Agency regional observation boreholes (2007–2010).

Fig. 2: (A) Extendable Dutch auger used for retrieving floodplain sediments. (B) An example of the floodplain sediment core after extraction using Dutch auger with lithology descriptions. (C) An example of retrieved riverbed sediment core using plastic tube with lithology descriptions (For core locations see Fig. 3)

Fig. 3: Study area with floodplain GPR profiles, in-channel GPR survey, and location of core logs and bank exposures. Floodplain Profiles 94–14, NE-SW orientations (solid black lines) are 50 m long and Profiles 15–20, NW-SE orientations (light grey lines) are varied between 100–132 m. In-stream GPR survey is 240 m. Orange and blue dots represent floodplain and riverbed core logs, respectively.

Fig. 4: Geological logs for auger holes retrieved from the floodplain (west bank site) during the GPR survey (see Fig. 3 for coring locations).

Fig. 5: (A) Riverbed lithology determined from core logs along the investigated study reach. (B) Locations of core logs on the map.

Fig. 6: (A) and (B) Sections of the ground truth (Bank exposure) control the profile. (C) GPR line 94 surveys collected close to the river bank, illustrating radar facies and ground truth validation with exposures. The type of sediments and sedimentary structures seen at the outcrop haven been used to establish the relationship between radar GPR reflections (e.g. subhorizontal versus dipping reflections) and sediments. The numbers indicate the different radar facies identified along the section. For a detailed description of each radar facies see the text and figure 8.

Fig. 7: Two examples (50 m long) (A) line 09 and (B) line 95 of NE-SW orientation GPR floodplain surveys, and (C) one example (126 m long) of NW-SE) orientation, illustrating numbered radar facies and calibration with core logs along the profile.

Fig. 8: Types of GPR reflections, their connection with ground truth data and interpretation, identified in the west bank (floodplain) river Tern study site.

Fig. 9: Quasi three-dimensional GPR profiles illustrating permeability class and radar facies distribution along west bank site of the river Tern. Green colours represent spatial distribution of channel elements filled by low permeability layers (low permeability field), while white colours represent channels filled by high permeability layers.

Fig. 10: Longitudinal in-channel survey (240m) showed GPR reflections, bathymetry, streambed topography, descriptions of bank exposures and core locations, lithology and structures of the riverbed.

Fig. 11: Three-dimensional block diagram for west bank floodplain sediment deposits.

Fig. 12: C.S. 5 core shows saturated area (high water level) which is caused by channel fill low conductivity materials in the study area (see Fig. 3 for core locations).

Table 1: Parameters setting during GPR measurements on floodplain (west bank site) river Tern site.

GPR parameters	Values
Frequency (MHz)	250
Survey type	Reflection
Time window (ns)	100
Units	m
Step size (m)	0.050
Antenna separation (m)	0.40
Odometer Cal (ticks/m)	1082.483

Stacks	8
Time sampling interval (ps)	400.000
Pulser voltage (V)	165

Table 2: Ground truth data presentation and relation to GPR profiles of the study area.

Ground-Truth data	Location and relation to the GPR profiles
Bank exposure 1	Located at the north of Heathbrook farm at the west bank. This exposure was correlated with GPR profile 94.
Bank exposure 2	Located at the north of Heathbrook farm at the west bank close to the meander bend. This exposure was correlated with GPR profile 94 as well.
Floodplain (C.S.1)	Retrieved at the intersection between GPR profile 94 and 15 at the start position.
Floodplain (C.S.2)	Retrieved at the intersection between 10 m position of GPR profile 16 and 95.
Floodplain (C.S.3)	Retrieved at the intersection between 30 m position of GPR profile 95 and 10 m of GPR profile 18.
Floodplain (C.S.4)	Retrieved at the intersection of 10 m of GPR profile 09 and GPR profile 16, position 60-62 m.
Floodplain (C.S.5)	Retrieved at the intersection of 90 m position of GPR profile 19 and 40 m position of GPR line 12.
Floodplain (C.S.6)	Retrieved at the intersection of the start position of GPR profiles 12,13,14 and end position of GPR survey 15.
Floodplain (C.S.7)	Retrieved at the position 20 m of GPR profile 13 and end of profile 16.
Riverbed (R.C.1)	Retrieved at 60 m position of GPR river profile.
Riverbed (R.C.2)	Retrieved at 90 m position of GPR river profile.
Riverbed (R.C.3)	Retrieved at the 110 m position of the longitudinal GPR profile.

Riverbed (R.C.4)	Retrieved at 125 m position of GPR profile.
Riverbed (R.C.5)	At 150 m of GPR profile (“hotspot”) location.
Riverbed (R.C.6)	At 155 m of the GPR profile.
Riverbed (R.C.7)	Around 170 m of the GPR profile.

Journal Pre-proof

Highlights

- We used a combination of novel in-stream GPR in conjunction with riparian surveys.
- Identifying the spatial patterns and extent of low conductivity structures in the streambed and riparian zone.
- The architectures of the fluvial settings have been found to control groundwater – surface water exchange fluxes and residence time distributions at the interface between aquifer and river.

Journal Pre-proof

A



B



C



Figure 2

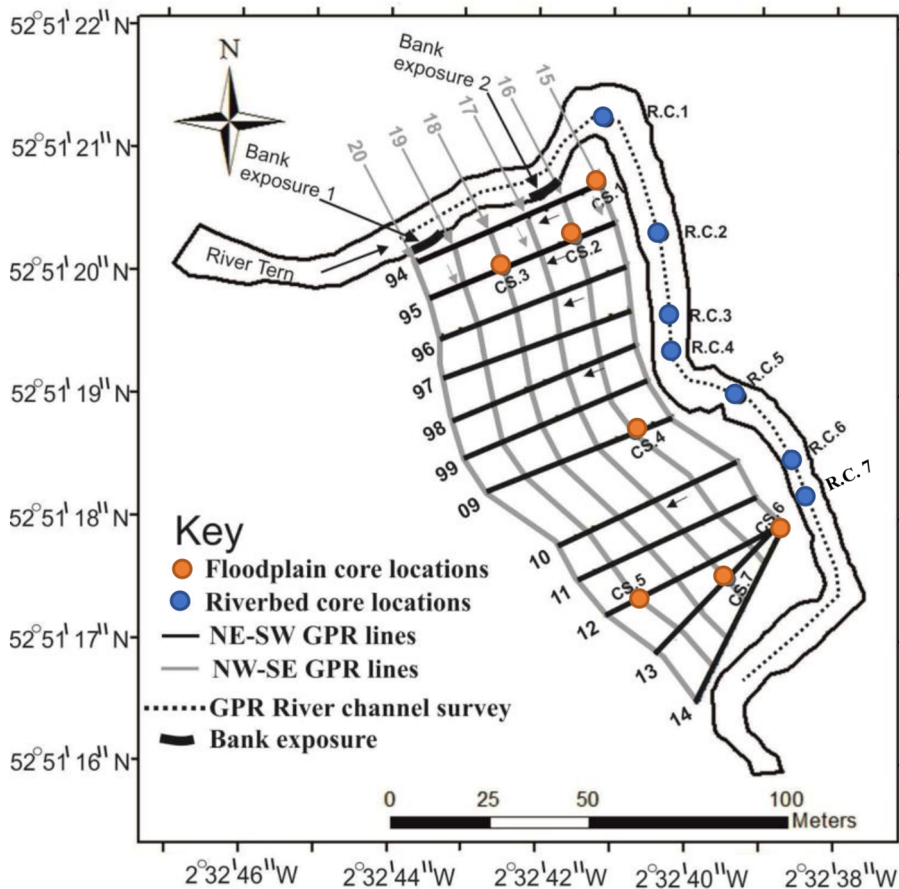


Figure 3

Floodplain cores

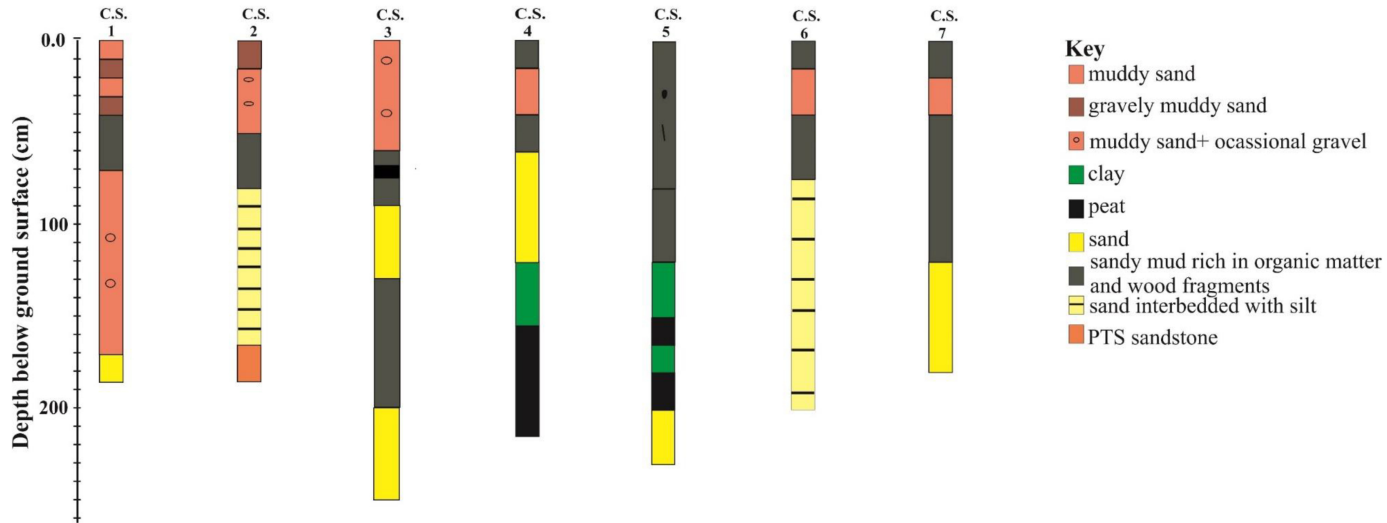
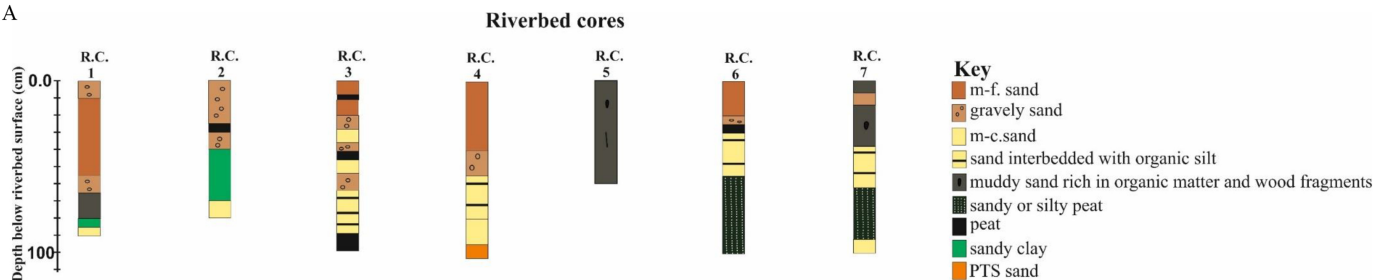


Figure 4

A



B

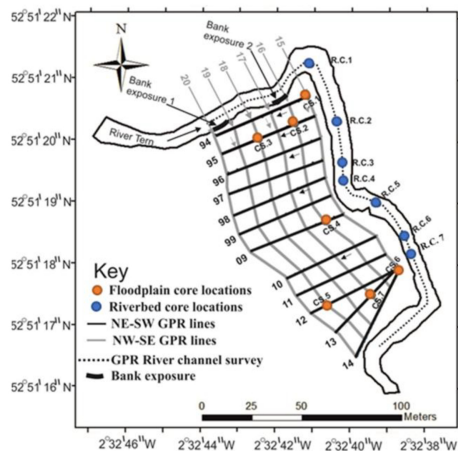


Figure 5

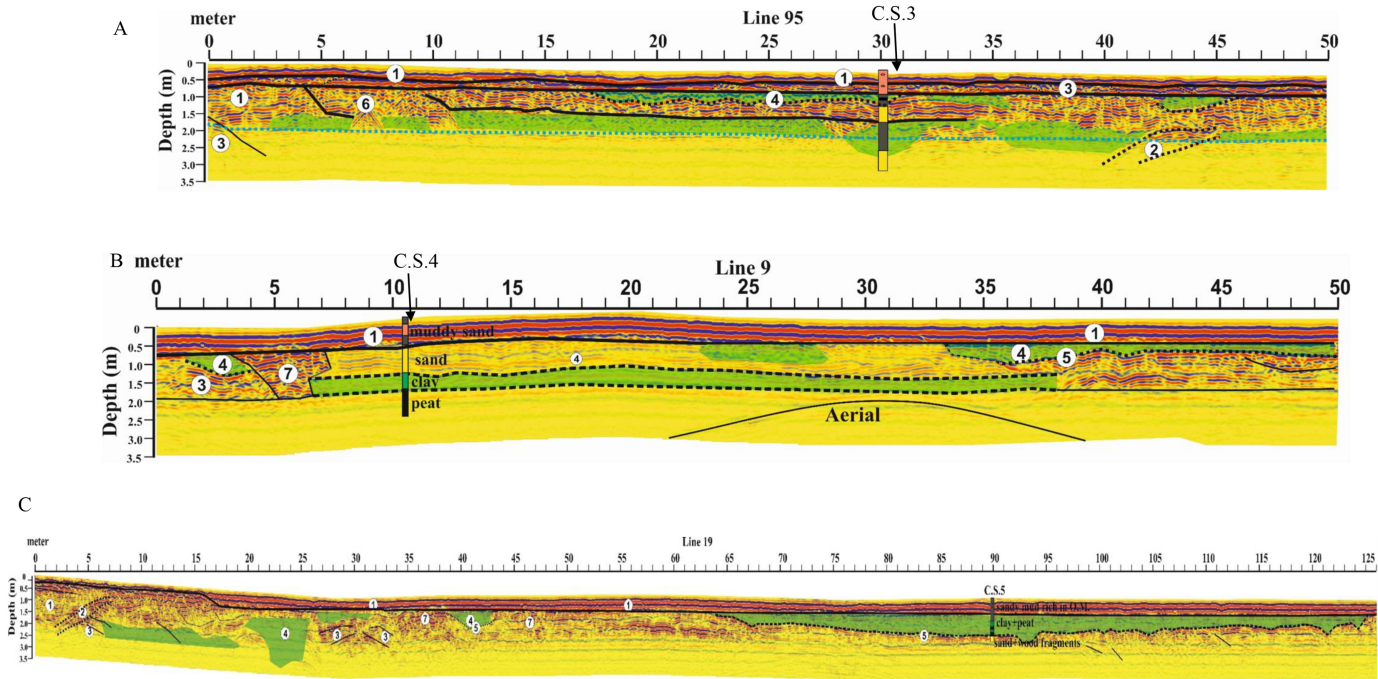


Figure 7

Radar facies	GPR example image	Core section	Lithology	Interpretation	Permeability class
Radar facies type 1 Horizontal-to-subhorizontal reflections			Fine muddy sand, plant remains, clay nodules, as well as some isolated pebbles	Overbank vertical accretion deposits	Intermediate
Radar facies type 2 Sigmoidal to divergent clinoform reflections			Sand layers interbedded with dark silt	Overbank flooding (modern floodplain)	High
Radar facies type 3 Wavy and Inclined reflections			Sand sediment	Lateral or downstream accretion and lateral migration of the river	High
Radar facies type 4 Faint subhorizontal, undular, variable dip, and structureless reflections			Muddy sand rich in organic matter, peat, and clay	Channel fill elements	Low
Radar facies type 5 Curved, concave-upward reflections associated with dipping and small hyperbolic reflections			Sand with organic fragments	Erosional surface	High
Radar facies type 6 Discontinuous, chaotic or irregular rich in macro scale abundant stacked hyperbolic reflections			Big boulders or bedrock surface	Deposits of submerged palaeomeander or bedrock	Low-High
Radar facies type 7 Hummocky, dipping and chaotic reflections including micro-scale hyperbolic diffractions.			Small boulders within sand deposits	Surrounding the older channels represent point bar sediment.	High
Radar facies type 8 Structureless, reflection free zone.			Clay layers	May correspond to swamp deposits	Low

Figure 8

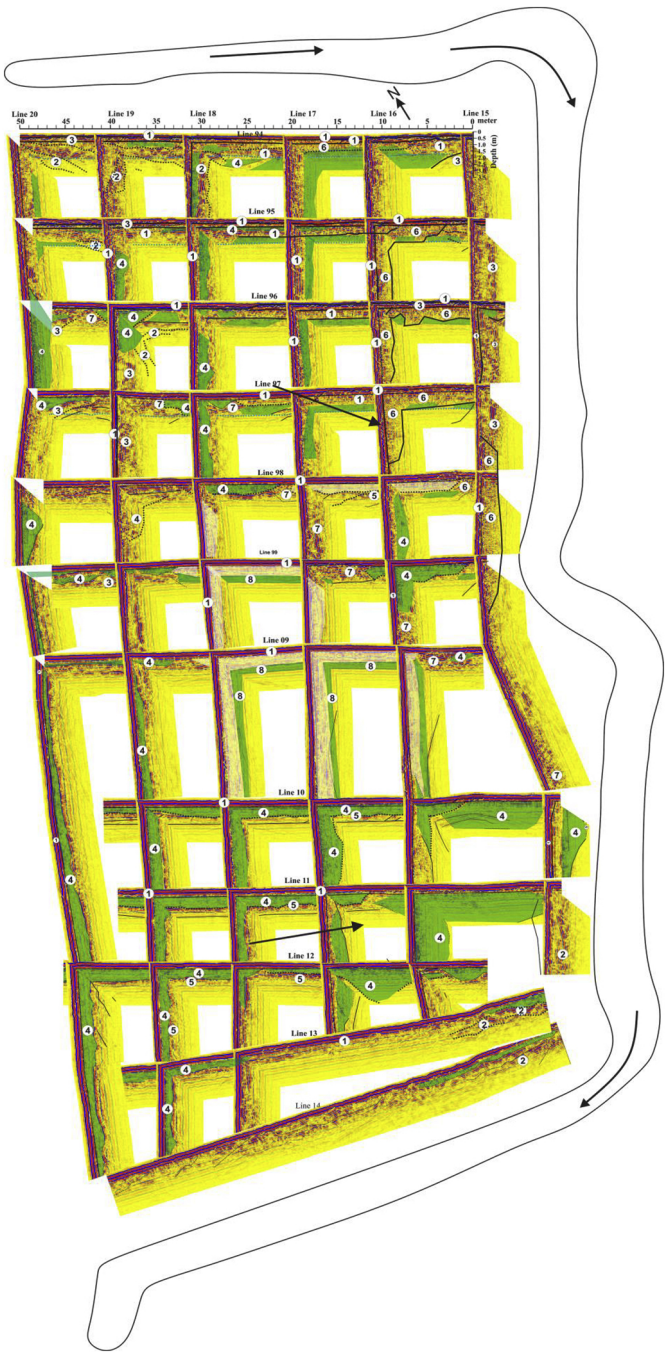
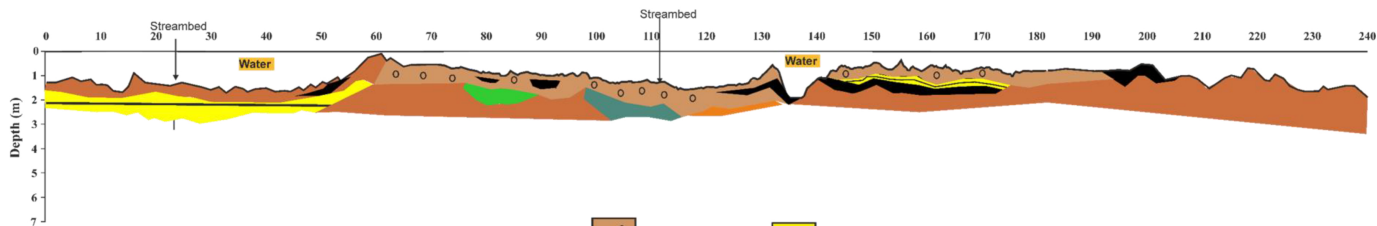
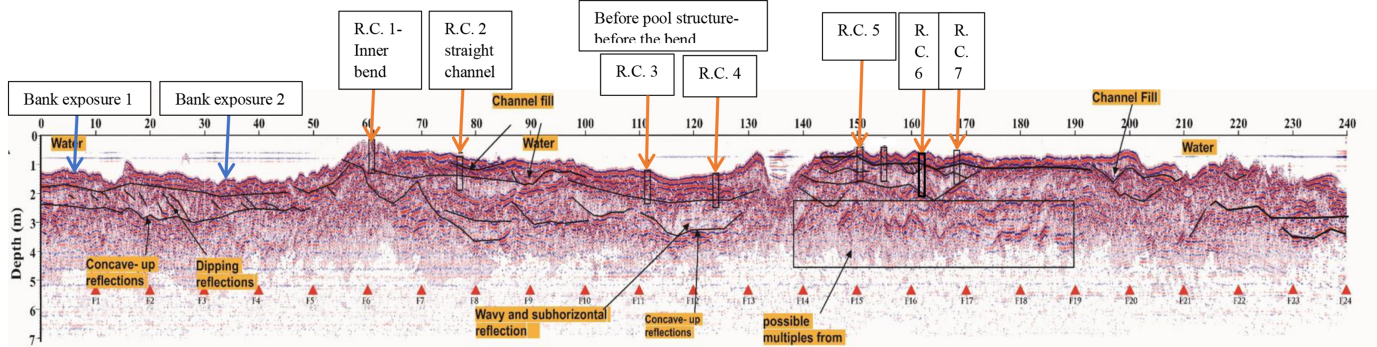
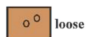








Figure 9



- | | | | |
|---|--------------------|---|--|
|  | loose sand, gravel |  | sand interbedded with silt, rich in OM |
|  | sand |  | peat |
|  | sandy, silty peat |  | PTS sand |
|  | sandy clay | | |



 Bank exposure locations
 River core sample locations

Figure 10

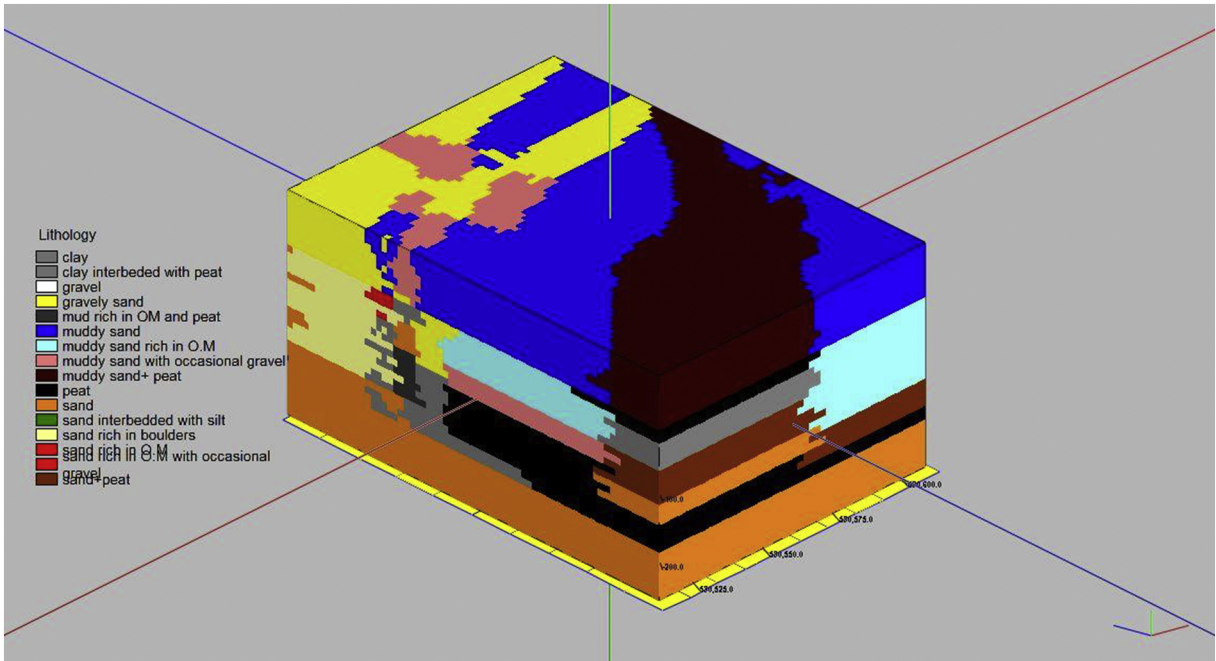


Figure 11



Figure 12